

An Engineering Approach to Thermal Margin Calculation Using Two-phase Boundary Layer Model

Ho-Jun Yoon, Kune Y. Suh

Seoul National University
San 56-1 Shinrim-dong, Kwanak-gu, Seoul, 151-742, Korea
Phone : +82-2-880-8281, Fax : +82-2-883-0827, Email : lager@plaza1.snu.ac.kr

Abstract

As an advanced in-vessel design concept, the COrium Attack Syndrome Immunization Structures (COASIS) are being developed as prospective in-vessel retention devices for a next-generation LWR in concert with existing ex-vessel management measures. Both the engineered gap structures in-vessel (COASISI) and ex-vessel (COASISO) were demonstrated to maintain effective heat transfer geometry during molten core debris attack when applied to the TMI-2 and the Korean Standard Nuclear Power Plant (KSNPP) reactors. This paper presents the first-principle calculation results for the thermal margin for the case of external cooling of the reactor vessel lower head. Adopting the method presented by F.B. Cheung, et al., we calculated the departure from nucleate boiling ratio (DNBR) for the three cases of pool boiling, flow boiling and subcooled boiling.

1. Introduction

Boiling has long been recognized as one of the most efficient ways of cooling hot or heated surfaces and that is of fundamental importance in many applications in the nuclear and chemical industries. However most of boiling research was focused on upward facing geometry and performed in the experiments using small objects. Thus there is a scarcity of data with direct applicability to cooling the hemispherical reactor lower head externally on a major scale. Recently, some studies did examine the external cooling of nuclear reactor vessel downward facing hemispherical surface.

Guo and El-Genk (1992) performed an experimental study of saturated pool boiling from downward facing and inclined surface. Pool boiling curves for inclinations of 0°, 5°, 10°, 15°, 30°, 45°, and 90° were obtained by quenching a 12.8mm thick copper disk having a diameter of 50.8mm in a pool of saturated water. Results showed that nucleate boiling heat flux decreases as angle of inclination is increased. However, the decrease in nucleate boiling heat flux with inclination is more pronounced at lower wall superheat, increasing with surface inclination.

El-Genk and Glebov (1995) studied transient pool boiling from downward-facing curved surfaces. In this study, quenching experiments were performed to investigate the effects of wall thickness on pool boiling from downward facing curved surfaces in water.

T.G Theofanous and Syri (1997) performed several external cooling experiments at the ULPU experimental facility. Their experiments are divided into configurations I, II, and III. Configuration I experiments established the lower limits of coolability under lower submergence, pool boiling conditions. Using configuration II experiments, they considered the heat flux shape, full submergence and natural circulation in the reactor lower head. They proposed the CHF correlation as follows

$$q''_{CHF}(\mathbf{q}) = 490 + 30.2\mathbf{q} - 8.88 \times 10^{-1}\mathbf{q}^2 + 1.35 \times 10^{-2}\mathbf{q}^3 - 6.65 \times 10^{-5}\mathbf{q}^4 \text{ kW/m}^2 \quad (1)$$

S. Rouge (1997) performed the SULTAN experiment to study large-scale structure coolability by water in boiling natural convection. The objective was to measure the main characteristics of two dimensional, two-phase flow so as to evaluate the recirculation mass flow in the large system. According to his result, the heat flux larger than 1MW /m² may be removed under natural water circulation conditions, provided that the water circuit is well designed and optimized.

Park & Jeong (1997) presented the thermal margin for external reactor vessel cooling in a large advanced light water reactor (ALWR). They chose Strinberner & Reineke (1978)'s Nusselt number for upward natural convection and Theofanous et al. (1995)'s Nusselt number and Mayinger et al. (1975)'s Nusselt number for the downward convection, respectively. They also cited the correlation based on Mini-ACOPO experimental data in order to find the angular heat flux distribution and calculated the CHF at the outer surface of the lower head using Theofanous et al.'s correlation (1995) developed from the ULPL-2000 configuration II experiment. Their results showed that the thermal margins were 27% and 64% depending on which correlation was used at the highest angle of the debris, i.e. $\theta = 85^\circ$.

2. Model Description

F.B. Cheung (1997) intended to establish a proper scaling law and develop a design correlation for prediction of the CHF on the exterior surface of a commercial-size reactor vessel. He analyzed the CHF by means of the theory of behavior of the micro-layer and two-phase boundary layer. After brief explanation of the theory, we demonstrate some typical numerical results from our application.

2.1 Occurrence of the Local CHF

The local rate of liquid supply, \dot{m}_s , from the two-phase boundary layer to the micro-layer is given by

$$\dot{m}_s = \rho_l u_l A_m \quad (2)$$

On the other hand, the local rate of depletion, \dot{m}_d , of the liquid film is given by

$$\dot{m}_d = q''_{NB} A_w / h_{fg} \quad (3)$$

here q''_{NB} is the heat flux in nucleate boiling.

Local dryout of the liquid film is considered to occur when the local rate of liquid supply becomes less than the local rate of liquid depletion. From equations (2) and (3), an expression for the local CHF, q''_{CHF} , can be obtained by setting \dot{m}_s equal to \dot{m}_d and q''_{NB} equal to q''_{CHF} , as

$$q''_{CHF} = r_l h_{fg} u_l \left(\frac{A_m}{A_w} \right) \quad (4)$$

Assuming the characteristic length of the vapor slug to be l , the net flow area A_m and the heating surface area A_w can be expressed by

$$A_m \sim (d_m)_{CHF} l \quad \text{and} \quad A_w \sim l^2 \quad (5)$$

From the two-phase boundary layer flow observation made in the SBLB experiments (Cheung, 1997), the characteristic length l is found to be proportional to the local two-phase boundary layer thickness, δ_0 , in the bottom center region, i.e.

$$l = C_4 d_0 \quad (6)$$

where C_4 is 4. Substituting equations (5) and (6) into equation (4), the following expression may be obtained for the local CHF:

$$q''_{CHF} = r_l h_{fg} u_l (d_m)_{CHF} / C_4 d_0 \quad (7)$$

2.2 Two-phase Boundary-layer Analysis

The momentum relation for the vapor-liquid mixture in the two phase boundary layer is governed by the following differential equation applicable to any location along the hemispherical heating surface:

$$\frac{d}{dq} \{ [r_g a u_g^2 + r_l (1-a) u_l^2] d \sin q \} = a d R g (r_l - r_g) \sin^2 q - (t_w - t_l) R \sin q \quad (8)$$

The wall and interfacial shear stresses are related by

$$t_w + t_l = 0.5 C_f [a u_g + (1-a) u_l] [r_g a u_g + r_l (1-a) u_l] \quad (9)$$

where C_f is a friction coefficient having the value of 0.005.

A mass balance on the liquid phase across the thickness of the two-phase boundary layer at any location gives

$$\frac{d}{dq}[(1-a)u_l \mathbf{d} \sin \mathbf{q}] = j_l R \sin \mathbf{q} \quad (10)$$

Similarly, a mass balance on the vapor phase across the thickness of the two-phase boundary layer under saturated boiling conditions at any location gives

$$\frac{d}{dq}[\mathbf{a}u_g \mathbf{d} \sin \mathbf{q}] = \frac{q''_{CHF} R \sin \mathbf{q}}{\mathbf{r}_g h_{fg}} \quad (11)$$

To close the system of the governing equations, an independent expression is needed for the relative velocity between the liquid and vapor phases. This is obtained by assuming that once the vapor mass departs from the heating surface, it would attain its terminal rise velocity relative to the liquid phase in the two-phase boundary layer. It then follows that

$$u_g = u_l + 1.53 \left[\frac{\mathbf{s}g \sin \mathbf{q} (\mathbf{r}_l - \mathbf{r}_g)}{\mathbf{r}_l^2} \right]^{1/4} \quad (12)$$

Inspection of equations (7) to (12) indicates that the following local boundary layer variables, namely, the dimensionless critical heat flux, Q_{CHF} , dimensionless boundary layer thickness, \mathbf{D} , dimensionless vapor velocity, U_g , and dimensionless liquid velocity, U_l , can be introduced to simplify the governing system of equations:

$$q''_{CHF} = \mathbf{r}_g h_{fg} \left[\frac{\mathbf{s}g (\mathbf{r}_l - \mathbf{r}_g)}{\mathbf{r}_g^2} \right]^{1/4} \left(1 + \frac{\mathbf{r}_g}{\mathbf{r}_l} \right)^{1/3} Q_{CHF} \quad (13)$$

$$\mathbf{d} = \left[\frac{\mathbf{s}R^2}{g (\mathbf{r}_l - \mathbf{r}_g)} \right]^{1/4} \left(\frac{\mathbf{r}_g}{\mathbf{r}_l} \right)^{-0.1} \mathbf{D} \quad (14)$$

$$u_g = \left[\frac{Rg (\mathbf{r}_l - \mathbf{r}_g)}{\mathbf{r}_g} \right]^{1/2} \left(\frac{\mathbf{r}_g}{\mathbf{r}_l} \right)^{0.1} U_g \quad (15)$$

$$u_l = \left[\frac{Rg (\mathbf{r}_l - \mathbf{r}_g)}{\mathbf{r}_l} \right]^{1/2} U_l \quad (16)$$

In terms of dimensionless local variables, we can summarize the above equations as follows

$$Q_{CHF} = B(U_l / \mathbf{D}_o)^{1/3} \quad (17)$$

$$\frac{d}{dq} \left\{ \left[\mathbf{a}U_g^2 + \left(\frac{\mathbf{r}_g}{\mathbf{r}_l} \right)^{-0.2} (1-a)U_l^2 \right] \mathbf{D} \sin \mathbf{q} \right\} = \mathbf{a} \mathbf{D} \sin^2 \mathbf{q} \left(\frac{\mathbf{r}_g}{\mathbf{r}_l} \right)^{-0.2} - 0.5 C_f L_b^{-1/2} \left(\frac{\mathbf{r}_g}{\mathbf{r}_l} \right)^{-0.2} \sin \mathbf{q} \\ \times \left[\mathbf{a}U_g + \left(\frac{\mathbf{r}_g}{\mathbf{r}_l} \right)^{-0.6} (1-a)U_l \right] \left[\mathbf{a}U_g + \left(\frac{\mathbf{r}_g}{\mathbf{r}_l} \right)^{0.4} (1-a)U_l \right] \quad (18)$$

$$\frac{d}{dq}[(1-a)U_l \mathbf{D} \sin \mathbf{q}] = J_l \left(\frac{\mathbf{r}_g}{\mathbf{r}_l} \right) L_b^{-1/2} \sin \mathbf{q} \quad (19)$$

$$\frac{d}{dq}[\mathbf{a}U_g \mathbf{D} \sin \mathbf{q}] = Q_{CHF} \sin \mathbf{q} \quad (20)$$

$$U_l = \left(\frac{\mathbf{r}_g}{\mathbf{r}_l} \right)^{-0.4} U_g - 1.53 (L_b^2 \sin \mathbf{q})^{1/4} \quad (21)$$

where

$$\mathbf{D}_o = \left[\frac{\mathbf{s}R^2}{g (\mathbf{r}_l - \mathbf{r}_g)} \right]^{-1/4} \left(\frac{\mathbf{r}_g}{\mathbf{r}_l} \right)^{0.1} \mathbf{d}_o \quad (22)$$

$$J_l = \left[\frac{Rg (\mathbf{r}_l - \mathbf{r}_g)}{\mathbf{r}_l} \right]^{-1/2} j_l \quad (23)$$

$$L_b = \frac{1}{R} \left[\frac{\mathbf{s}}{g (\mathbf{r}_l - \mathbf{r}_g)} \right]^{-1/2} \quad (24)$$

We solved the above equations for hemispheres of diameter 4m and 0.5m, using the Runge-Kutta method, the Newton-Raphson method and the implicit method.

2.3 Application to COASISO

Based on the previous model, we find out local CHF, vapor velocity, liquid velocity, boundary layer thickness for 0.5 and 4m diameter hemispherical vessels in pool boiling, forced convection and subcooled boiling. Utilizing the previous model, we must assume the CHF values from 0° to 5° as constant in solving the initial dimensionless boundary thickness. We assumed the value of 0.4 MW/m² according to the SBLB experiment (Cheung, 1997). For all experimental studies carried out so far, we assumed that heat flux from the debris bed in the reactor vessel lower head to the outside wall varies azimuthally. For years, a number of investigators have studied the heat flux from the debris to the reactor vessel lower head. They concentrated on several natural convection experiments in the lower head vessel. Table 1 is a summary of the major experiments in the scaled vessel. In these experiments, the Rayleigh number, Ra', is defined as follows:

$$Ra' = \frac{g \beta Q_c H^5}{k_p \alpha_p \nu_p}$$

Table 1. Summary of the major natural convection experiments

Experiment concept	Scale/Shape Dimensionality	Working Fluid	Ra'
UCLA Microwave heating	1/8 Hemispherical Axisymmetric	Freon-113	$4 \cdot 10^{11} \sim 1 \cdot 10^{14}$
Mini-ACOPO Cooldown	1/8 Hemispherical Axisymmetric	Freon-113 Water	$2 \cdot 10^{13} \sim 7 \cdot 10^{14}$ $1 \cdot 10^{11} \sim 3 \cdot 10^{12}$
Jahn & Reineke	Semicircular	Water	$5 \cdot 10^5 \sim 1 \cdot 10^8$

In this study, we need the correlation of the experimental data for the heat transfer coefficient varying with the local position. Several investigators proposed correlations based on the experimental data, some of which are compared in figure 1. According to figure 1, respective correlations have essentially the same trend, but Park & Dhir's correlation and Suh & Henry's correlation did not fit the experimental data of Jahn & Reineke's (1974) adequately. We corrected Suh & Henry's correlation: by replacing constant 8 in the parenthesized numerator with 12. So we utilized Suh & Henry's corrected correlation to input the data of the actual heat flux values. The graphical comparison of Jahn & Reineke's experimental data, Suh & Henry's correlation and the new correlation are showed in figure 2.

Next, we must choose the fraction of heat transferred to the downward-facing wall. Among the research on heat removal, the COPO experiment reported on the fraction of heat transfer to the upward, sideward and downward-facing walls, respectively. According to table 2, the fraction of heat removal to the downward surface was about 13%. For conservatism's sake, however, the average heat flux was calculated assuming that the decay heat was 0.7% of nominal operating power of which 30% or 50% was transferred to the downward surface, respectively. The reason we chose the value of 0.7% is to obtain the thermal margin after the time has elapsed that the debris had accumulated and solidified in the reactor lower head vessel. Nominal operating power considered is only 4000MWt in this study.

Table 2. The split of total heat generation

Experiment	Ra	Up(%)	Side(%)	Down(%)
COPO	1.3×10^{15}	70	16	14
	1.5×10^{15}	76	13	11

3. Results and Discussion

3.1 Pool Boiling

The conceptual design of a COASISO device is illustrated in figure 3 as proposed by Hwang et al. (1998). As the gap between the reactor lower head and the inner wall of the COASISO structure will exceed the two-phase boundary layer thickness in pool boiling, we can apply previous model to

COASISO to calculate the thermal margin.

According to figures 4, 5, 6 and 7, the trend of results for the CHF, boundary layer thickness and velocities of liquid and vapor is similar to Cheung's results. Figure 8 is the calculated thermal margin for 4000MWt nominal operating power in pool boiling. According to the results, the thermal margin is the highest at the lower region for the cases considered. Despite increase of the removable energy moving from the bottom to the top, the reason the DNBR decreases is that emitted heat flux also increases moving from the bottom up. In case that 30% of the decay heat was transferred to the downward surface, we have larger thermal margin than minimum DNBR 1.3 even at the top. However, referring to the figure 9, thermal margin can vary dependent on using correlation. For higher fraction of the decay heat transferred to the downward surface, thermal margins were not enough to guarantee structural thermal integrity of the lower head.

3.2 Forced Convection

In order to quantify the effect of forced convection, we added the liquid velocity (3m/s, 10m/s) to the liquid velocity in the boundary layer at saturated pool boiling. The reason that we increased the liquid velocity is that the amount of removal heat is proportional to the liquid mass flow rate. The boundary layer thinning effect is not considered in this study. The result demonstrates that the forced convection has the effect of increasing the CHF in the bottom area. As the coolant flows from the bottom up, the flow area increases which in turn causes the flow to decelerate so that the forced circulation effect diminishes in the upper region of the COASISO structure. Hence the liquid velocity in the upper region has little difference than that of pool boiling. The liquid velocity in the boundary layer increases linearly flowing upward, while the injected liquid velocity decreases, hence the entire liquid velocity has the shape of figure 10, and the CHF has the same shape.

Figure 11 is the graphical comparison of the thermal margin. As we can see, the thermal margins in the lower areas are increasing while the trends in the upper areas are more or less similar to pool boiling.

3.3 Subcooled Pool Boiling

In order to investigate the effect of subcooling, we used Ivey and Morris's correlation (1962) given by

$$q''_{CHF} = q''_{CO} \left[1 + 0.102 \left(\frac{r_1}{r_g} \right)^{0.75} c_{pl} \frac{\Delta T_{sub}}{h_{fg}} \right] \quad (25)$$

The above equation was modified from Kutateladze's equation to agree well with the experimental data for water, ethly alcohol, ammonia, carbon tetrachloride, and isooctane over the pressure range from 0.0276 to 3.44 MPa. When we considered the subcooling effect, the CHF values increased in the upper region depending on ΔT_{sub} (see figure 12). The thermal margin results are summarized in figure 13. When we compare the CHF value for the 10°C subcooled water with that for the saturated water, the thermal margin increases about 48% at the top. We thus can secure a safe thermal margin when 30% of the decay heat is transferred and working fluid temperature is 90°C. But we lack the thermal margin when 50% of the decay heat is transferred.

3.4 Subcooled Forced Convection

According to figure 14, the CHF of the lower region increased by the forced convection effect and that of the upper region increased by the subcooling effect. The CHF can be enhanced over the whole lower head taking advantages of both the forced convection and subcooling effects. The results are plotted in figure 15. By considering both effects at the same time, we obtained higher thermal margin over the entire region. But we could not ensure safety at the top when 50% of the decay heat was transferred. Figure 15 is the maximum margin and minimum margin that we can maintain by considering the effects of forced convection and subcooled boiling. Now we know that the effect of the subcooled forced convection enhance thermal margin. So the conceptual diagram in figure 3 can be modified as in figure 16, if it is desirable.

4. Conclusion

According to this study, we may jeopardize the thermal margin at the top in the very severe case that 50% of the decay heat is transferred to the downward surface. However, this assumption might as well be overly conservative. As we mentioned previously, the fraction of removal heat to the downward surface is about 13% of the total decay power. Hence the cases that 30% of the decay heat is transferred to the downward surface should already be conservative. Thus it is concluded that we may possibly guarantee safe thermal margin for a great deal of cases studied in this work.

To further increase the thermal margin, we may partly inject the water directly to the middle angular region so as to maximize the effect of forced convection starting over from the middle region.

REFERENCES

- Asfia F. J. and Dhir V. K. (1994), An experimental study of natural convection in a volumetrically heated spherical pool with rigid wall, International Mechanical Engineering Congress & the Winter Annual Meeting, Chicago, Illinois, November 6-11
- Cheung F. B., Haddad K. H. and Liu Y. C. (1997), Critical heat flux phenomenon on a downward facing curved surface, *NUREG/CR-6507 PSU/ME-97-7321*
- El-Genk M. S. and Glebov A.G. (1995), Transient pool boiling from downward-facing curved surface, *Int. J. Heat Mass Transfer*, vol. 38, no. 12, pp. 2209-2224
- Guo Z. and El-Genk M. S. (1992), An experimental study of saturated pool boiling from downward facing and inclined surfaces, *Int. J. Heat Mass Transfer*, vol. 35, no. 9, pp. 2109-2117
- Hwang I. S., Suh K. Y., Jeong K. J., Lim D. C. and Park S.D. (1998), In-vessel retention against water reactor core melting accidents, submitted for publication in *Nuclear Engineering and Design*.
- Ivey H. J. and Morris D. J. (1962), On the relevance of the liquid-vapor exchange mechanism for subcooled boiling heat transfer at high pressure, *UKAEA, AEEW-R 137*
- Jahn M. and Reineke H.H. (1974), Free convection heat transfer with internal heat sources, Proceedings of the Fifth International Heat Transfer Conference, vol. 3, p. 74
- Marcus B. D. and Dropkin D. (1963), The effect of surface configuration on nucleate boiling heat transfer, *Int. J. Heat Mass Transfer*, vol. 6, pp. 863-867
- Mayinger F., Jahn M, Reineke H.H. and Steinberner U. (1975), Examination of thermohydraulic process and heat transfer in a core melt, Final report BMFT RS 48/1, Technical University, Hannover, Germany
- Nishikawa K., Fujita Y., Uchida S. and Ohta H. (1983), Effect of heating surface orientation on nucleate boiling heat transfer, ASME-JSME Thermal Eng. Joint Conf., vol 1, pp. 129-136
- Park H. J., Dhir V. K. and Kastenberg W. E. (1994), Effect of external cooling on the thermal behavior of aboiling water reactor vessel lower head, *Nuclear Technology*, vol. 108, pp. 266-282
- Park J. W. and Jeong D. W. (1997), An investigation of thermal margin for external reactor vessel cooling (ERV) in large advanced light water reactor (ALWR), Proceedings of the Korean Nuclear Society Spring Meeting, Kwangju, Korea, vol 1, pp. 473-478
- Rouge S. (1997), SULTAN test facility for large scale vessel coolability in natural convection at low pressure, *Nuclear Engineering and Design*, vol. 169, p. 185
- Steinberner U. and Reineke H. H. (1978), Turbulant buoyancy convection heat transfer with internal heat sources, Proc. Sixth Int. Heat Transfer Conference, Toronto, Canada, August
- Suh K. Y. and Henry R. E. (1994), Integral analysis of debris material and heat transport in reactor vessel, *Nuclear Engineering and Design*, vol. 151, pp. 203-221
- Theofanous T.G. et.al (1995), In-vessel coolability and retention of a core melt, *DOE/ID-10460*, vol 1, U.S. Department of Energy
- Theofanous T.G. and Syri S. (1997), The coolability limits of a reactor vessel lower head, *Nuclear Engineering and Design*, vol. 169, pp. 59-76

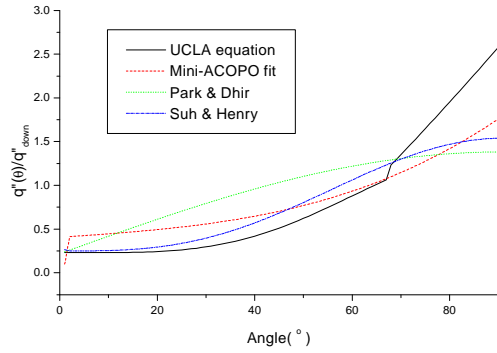


Fig 1. Graphical comparison of the natural convection correlations

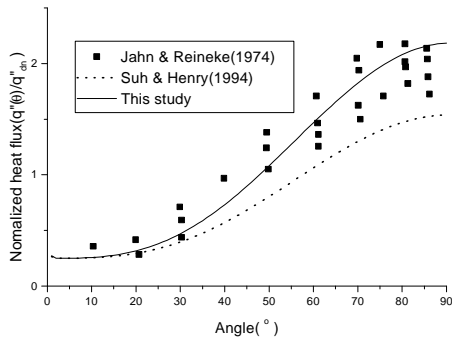


Fig 2. New fitting correlation of the data of Jahn & Reineke

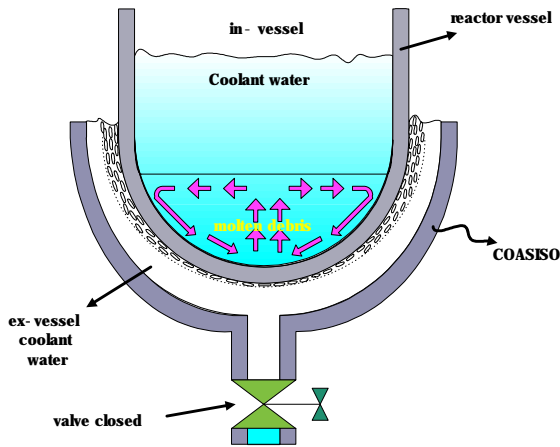


Fig 3. The conceptual design for COASISO with pool boiling

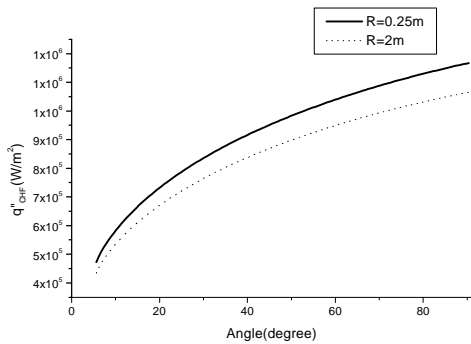


Fig 4. Critical heat flux in pool boiling

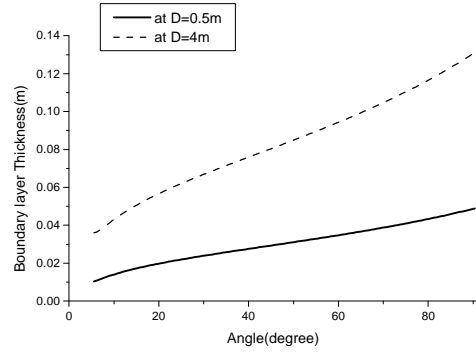


Fig 5. Boundary layer thickness in pool boiling

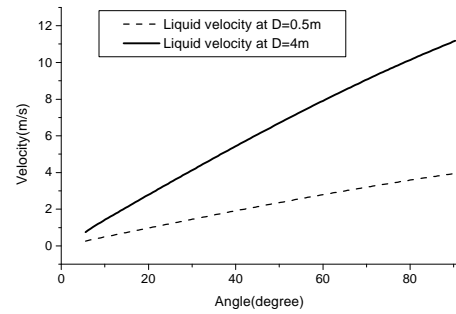


Fig 6. Liquid velocity in boundary layer in pool boiling

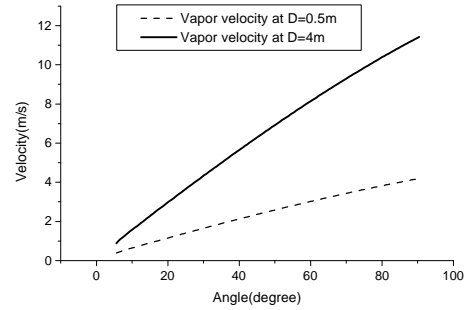


Fig 7. Vapor velocity in boundary layer in pool boiling

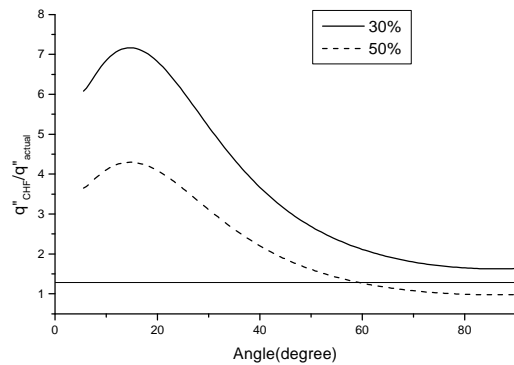


Fig 8. Thermal margin in pool boiling in case that 30% and 50% of the decay heat is transferred to the downward surface

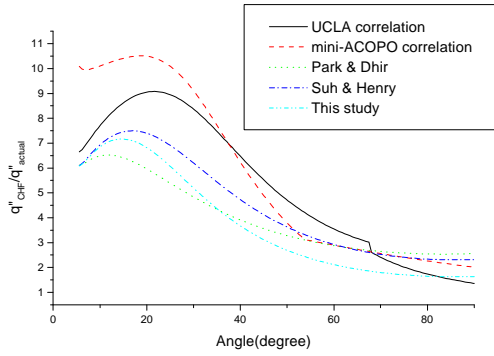


Fig 9. Comparison of thermal margin for several correlations

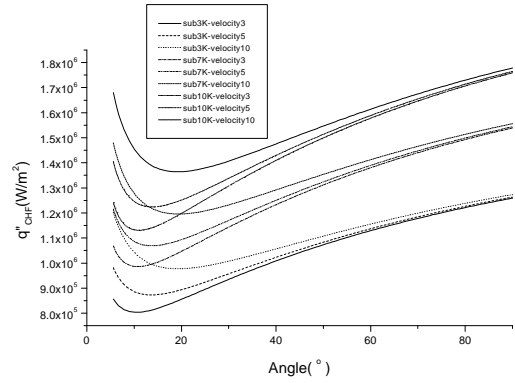


Fig 14. Critical heat flux in subcooled forced convection

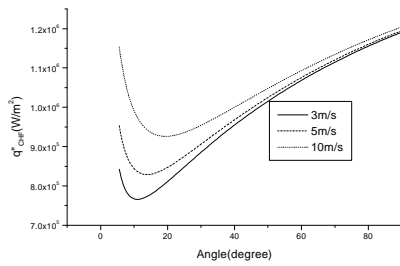


Fig 10. Critical heat flux in forced convection

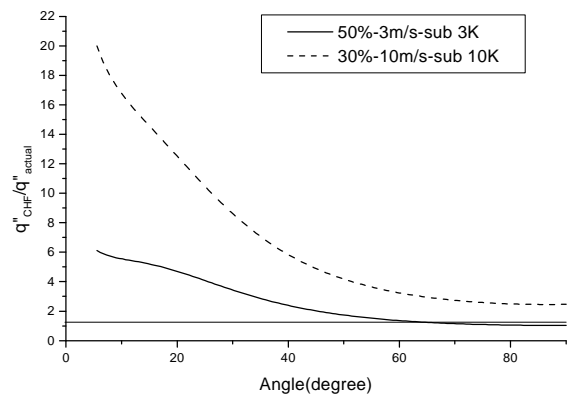


Fig 15. Thermal margin in subcooled forced convection in case that 50% of the decay heat is transferred to the downward surface, ΔT_{sub} is 3K and inlet velocity is 3m/s

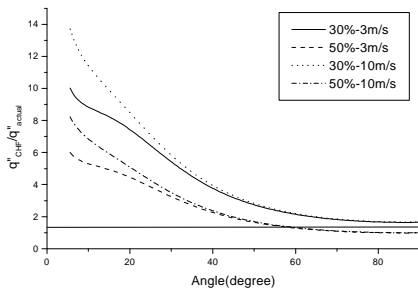


Fig 11. Thermal margin in forced convection

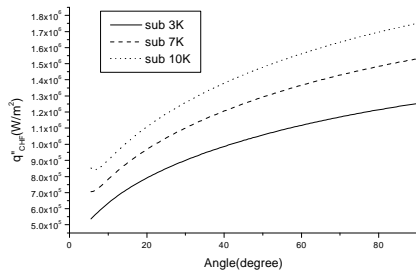


Fig 12. Critical heat flux in subcooled pool boiling

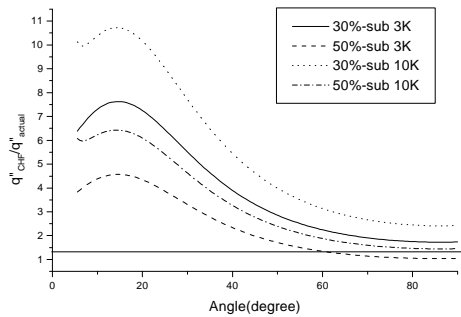


Fig 13. Thermal margin in subcooled pool boiling

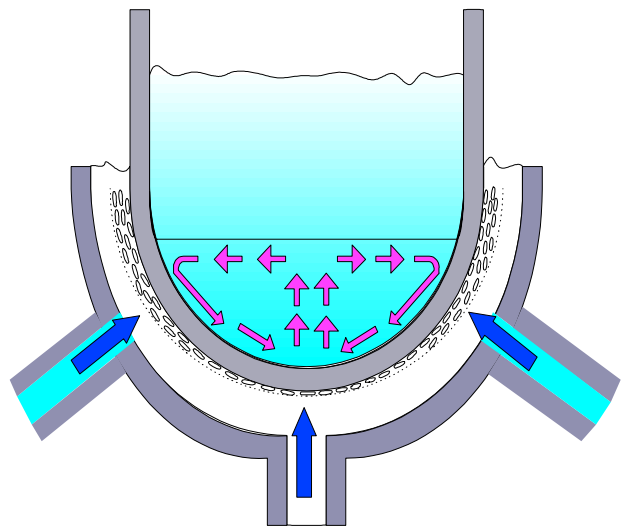


Fig 16. Conceptual design of COASISO with subcooled forced convection boiler

